Hindawi
International Journal of Aerospace Engineering
Volume 2023, Article ID 1477251, 18 pages
https://doi.org/10.1155/2023/1477251

Research Article

Effects of the Shock Wave Structure on the Tip Clearance Leakage Flow in Transonic Compressor Rotors

Xinlong Ye and Zhenggui Zhou

Jiangsu Province Key Laboratory of Aerospace Power Systems, Nanjing University of Aeronautics and Astronautics, Nanjing 210016, China

Correspondence should be addressed to Zhenggui Zhou; zzgon@nuaa.edu.cn

Received 14 September 2022; Revised 21 October 2022; Accepted 20 January 2023; Published 20 February 2023

Academic Editor: Dakun Sun

The interaction between shock waves and the tip clearance flow in a transonic compressor rotor has important effects on the tip clearance flow and the rotor aerodynamic performance. In this paper, two transonic rotors with a high pressure ratio are selected to study the tip flow, one of which has one normal shock wave at the blade tip and the other has two shock waves (an oblique shock wave and a normal shock wave) at the tip. The two rotors have the same meridional flow channel, design point flow rate, pressure ratio, and rotation speed to focus on the influence caused by the effect of the shock wave structure. The numerical results for the flow fields show the following conclusions. The strength of the two shock waves at the blade tip is weaker than that of one normal shock, and the former two shock waves are less stable than the latter. Therefore, with increasing tip clearance, the efficiency, pressure ratio, and stall margin of the rotor with the two shock waves decrease more rapidly. The static pressure difference between the pressure and suction sides of the tip clearance is the only driving factor of the tip clearance leakage flow, and the leakage flow depends on the local pressure difference and the secondary leakage caused by adjacent blades. The movement speed of the annular wall is less than that of the leakage flow, which has a minor blocking effect on the tip clearance leakage flow. The change in tip clearance has little effect on the chordal distribution of the static pressure difference and leakage flow rate per unit area, so the total leakage flow varies linearly with the tip clearance size.

1. Introduction

Tip clearance flow and its mixing with main flow and spanwise transport flow, including the interaction with shock waves in supersonic or transonic rotors, form a complex three-dimensional flow [1]. Studies show that the flow loss in the tip region accounts for approximately one-third of the total loss of the compressor, so the rotor tip region is a high loss region, usually also the stall initiation region [2–7]. The tip region of the rotor is the only region with high flow loss regardless of whether the pressure ratio is high or low [8, 9]. The higher the rotor pressure ratio and the larger the tip clearance, the higher the flow loss in this region. In addition, tip leakage flow is also an important self-noise source [7, 10, 11].

The effect of tip clearance on the performance of the compressor rotor of stage 9 of a 13-stage large IGT (industrial gas turbine) was studied using numerical simulations by Sakulkaew et al. [12]. The result shows three trends of efficiency variation with tip clearance. For a small tip clearance (<0.8% span), the trend of efficiency variation is nonmonotonic with an optimum tip clearance for maximum efficiency. The optimum gap exists because the trend of tip leakage mixing loss and viscous shear loss is opposite with increasing tip clearance. For a middle tip clearance (0.8%–3.4% span), the efficiency is monotone linear decreasing with increasing tip clearance. For a large tip clearance (>3.4% span), the change of tip clearance has no effect on efficiency due to the aft-loaded at the blade tip. The studies in references [13–15] show a similar trend.

Table 1: Main parameters of the two rotors.

Parameters	Design values	
	Rotor37	RotorSD
Number of blades	36	
Rotational speed (rpm)	17188	
Tip speed (m/s)	454	
Tip clearance (mm)	0.356	
Mass flow rate (kg/s)	20.19	
Total pressure ratio	2.10	
Isentropic efficiency	0.868	0.907
Surge margin (%)	14.0	15.4

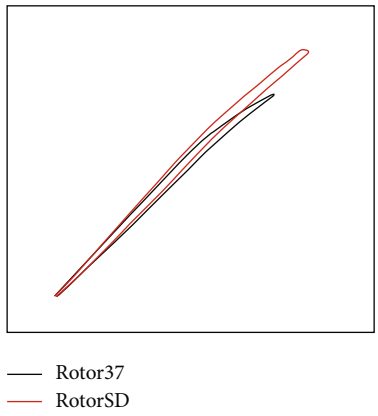

Figure 1: Comparison of the geometry of the two rotors at 90% span.

The change in tip clearance affects not only the rotor performance but also the downstream stator performance and the stability of the stage [15–18]. Howard and Puterbaugh [19] combined computational fluid dynamics(CFD) unsteady simulation calculations and experiments to study the effect of the tip clearance variation on the efficiency of the transonic small aspect ratio (average rotor aspect ratio = 0.57) axial compressor stage. The results show that the flow rate, pressure ratio, and efficiency are reduced when the tip clearance is increased and that spanwise transport and/or mixing occur within the downstream stator, which causes an increase in the loss of the stator. Liu et al. [20] studied about the effect of the rotor tip clearance variation on performance of downstream stator of a highly loaded compressor stage by using oil flow visualizations, stereoscopic particle image velocimetry (SPIV), and five-hole probe measurements. The result shows that a critical rotor tip blockage usually occurs at a certain rotor tip clearance configuration, resulting in more fluid moving to the low blade region, which causes an increase in loading at the hub and a decrease in the tip corner separation of the rotor, and the opposite is true for the stator.

More recent research was performed in the field of tip clearance leakage flow field structure and flow mechanism, which were the basis of understanding the effect of the tip clearance on compressor performance [21, 22]. The tip clearance flow of Rotor37 rotor was simulated and compared with the experiment by Chima [23]. The results show that there are three

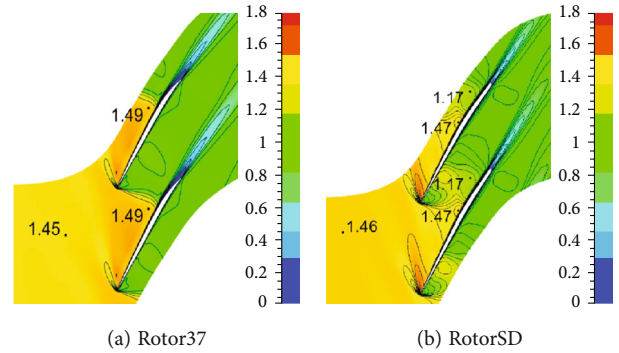

(a) Rotor37 (b) RotorSD

Figure 2: Contours of the relative Mach numbers at 90% span.

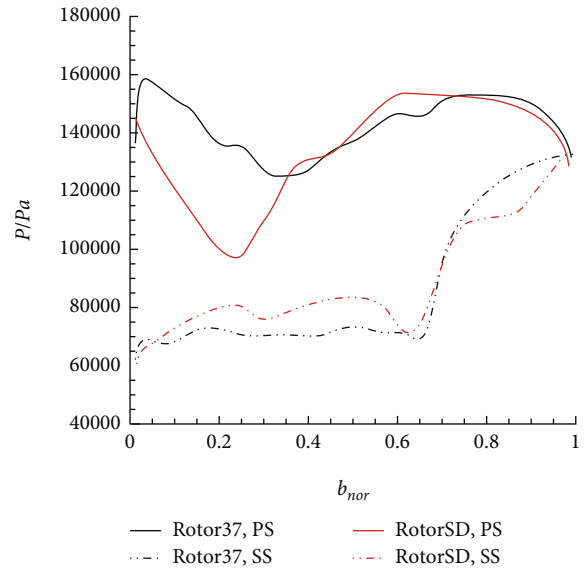

Figure 3: Static pressure distribution of two rotors at 90% span.

regions of different loads: a small, highly loaded region near the leading edge produced a strong clearance vortex; a large, moderately loaded region between the leading edge and the shock produced a wall jet; and a lightly loaded region downstream of the shock passed the clearance flow with little effect. Hoeger et al. [24] studied the inlet stage of a high-pressure compressor and found that there is obvious interaction between the tip leakage vortex and the shock wave in a transonic axial compressor, which greatly reduces the compressor efficiency and stability margin. Zhang et al. [25] measured the flow structure in tip region in a large-scale low-speed axial compressor and found a breakdown of the tip leakage vortex at the near stall condition for both of two tip clearances. And Wang et al. [26] found the breakdown of tip leakage vortex occurs in an intermittent manner. The tip leakage vortex (TLV) in a mixed flow pump as turbine at pump mode is decomposed and reconstructed by dynamic mode decomposition (DMD) by Liu and Tan and Han and Tan [27, 28]. The results show that the primary tip leakage vortex (PTLV) can be mainly classified as two parts, oscillating PTLV-A and shedding PTLV-B. PTLV-A starts near the blade leading edge and propagates downstream the passage with obvious oscillation, while PTLV-B

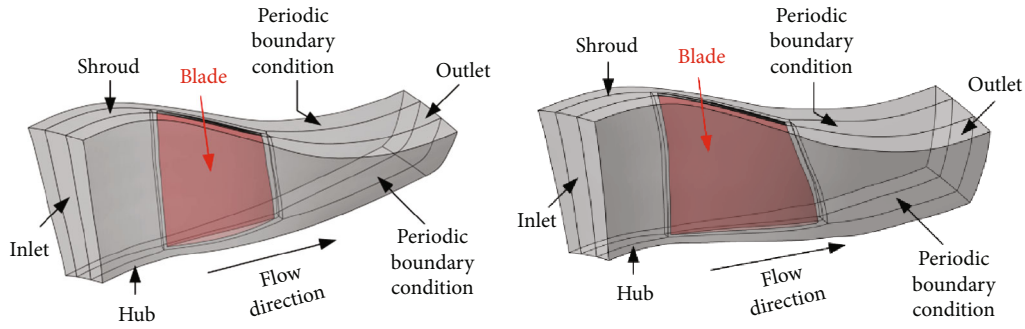

(a) Rotor37 (b) RotorSD

Figure 4: Computational domain.

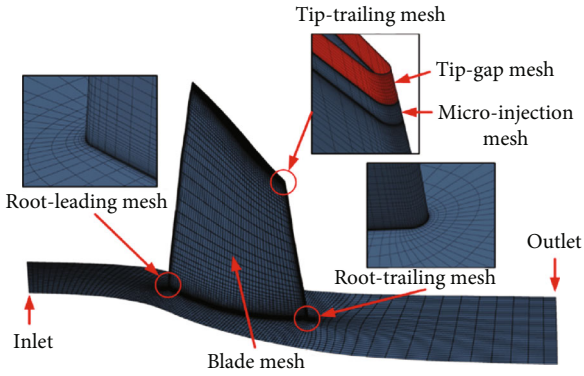

Figure 5: Schematic diagram of the grid.

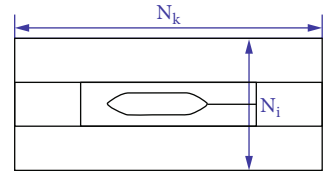

Figure 6: O4H topology.

Table 2: Number of grid points.

Grid points	N_i	N_j	N_k
290,000	41	57	109
390,000	49	65	109
500,000	57	73	109
610,000	65	81	109
750,000	69	85	109

stretches from the leading edge firstly and then sheds downstream. And the tip clearance has a slightly effect on the separation point of the PTLV but no effect on the separation angle.

In this paper, the flow field of two transonic high pressure ratio compressor rotors with different shock wave structures at the blade tip is numerically calculated, the effect of different shock wave structures on the tip clearance flow is studied, and finally, the driving factors of the tip clearance flow are presented.

2. Two Transonic Rotors with Different Shock Wave Structures

In this paper, two transonic compressor rotors are studied: NASA Rotor37 and RotorSD designed by our own research group. The meridional channels of the two rotors are the same, and the design mass flow, total pressure ratio, and rotating speed are also the same, as shown in Table 1. The tip profiles of the two rotors are shown in Figure 1. It shows that compared with Rotor37, the chord length of the RotorSD tip profile is longer and the curvature of the rear part is smaller. The relative Mach number contours at the 90% span of the two rotors at the design point are shown in Figure 2. From Figure 2, it can be seen that there is a single normal shock wave at the blade tip of Rotor37 and that there are one oblique and one normal shock wave at the tip of RotorSD. The profile at the blade tip of Rotor37 is foreloaded, and the load in front of the profile of RotorSD is low, as seen in Figure 3.

3. Computational Setup

The commercial NUMECA software is used to calculate the flow fields (see Figure 4), and the flow fields are simulated using three-dimensional steady Reynolds-averaged Navier-Stokes (RANS) equations with the Spalart-Allmaras (S-A) turbulence model. The spatial second-order upwind difference scheme is used to discretize the governing equations. Boundary conditions are specified to match the conditions of the experiment in the literature. The inlet boundary condition is set to 288.15 K for the total temperature and 101325 Pa for the total pressure and axial for the velocity direction. The outlet boundary condition is set to the radial equilibrium equation, and the static pressure at root is given. No-slip boundary condition is used on the hub, shroud, and blade surface.

The AutoGrid5 software is used to generate a grid, and the distance from the first grid to the wall is given as 2×10^{-6} m($y+ \approx 1$) according to the Blasius equation. The O4H topology is used on the S_1 surface, which is composed of an O-grid on the blade surface and four H-grids. The computational domain and three-dimensional topological structure of the grids of the two rotors are identical, as shown in Figures 5 and 6. To examine the dependence of the calculation results on the number of grid cells, five grids are generated, as shown in Table 2, in which N_i and N_k are the number of streamwise direction and azimuthal nodes,

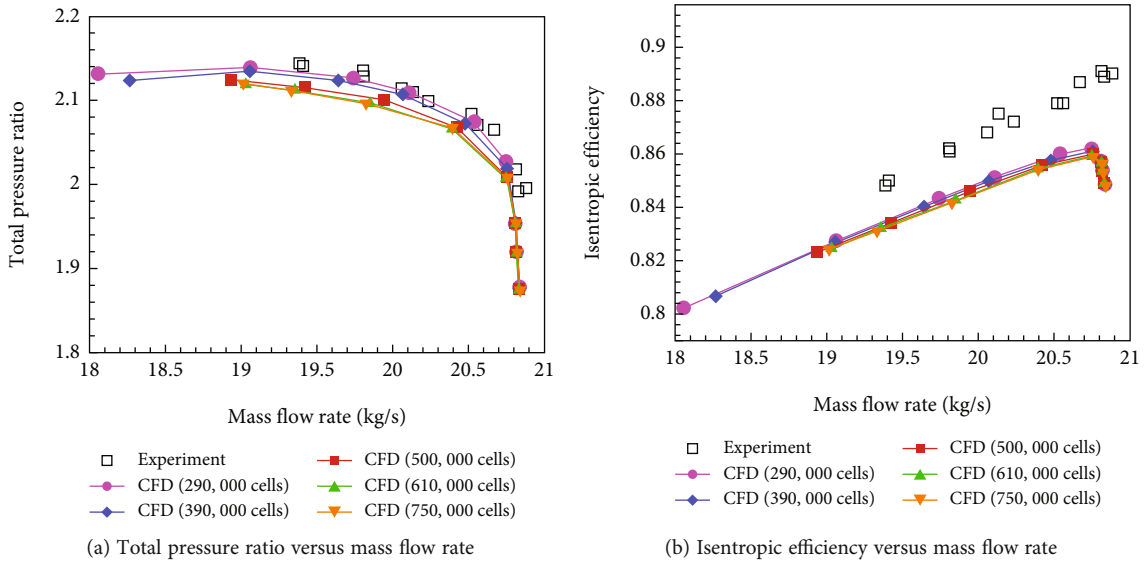

(a) Total pressure ratio versus mass flow rate

(b) Isentropic efficiency versus mass flow rate

Figure 7: Performance of NASA Rotor37.

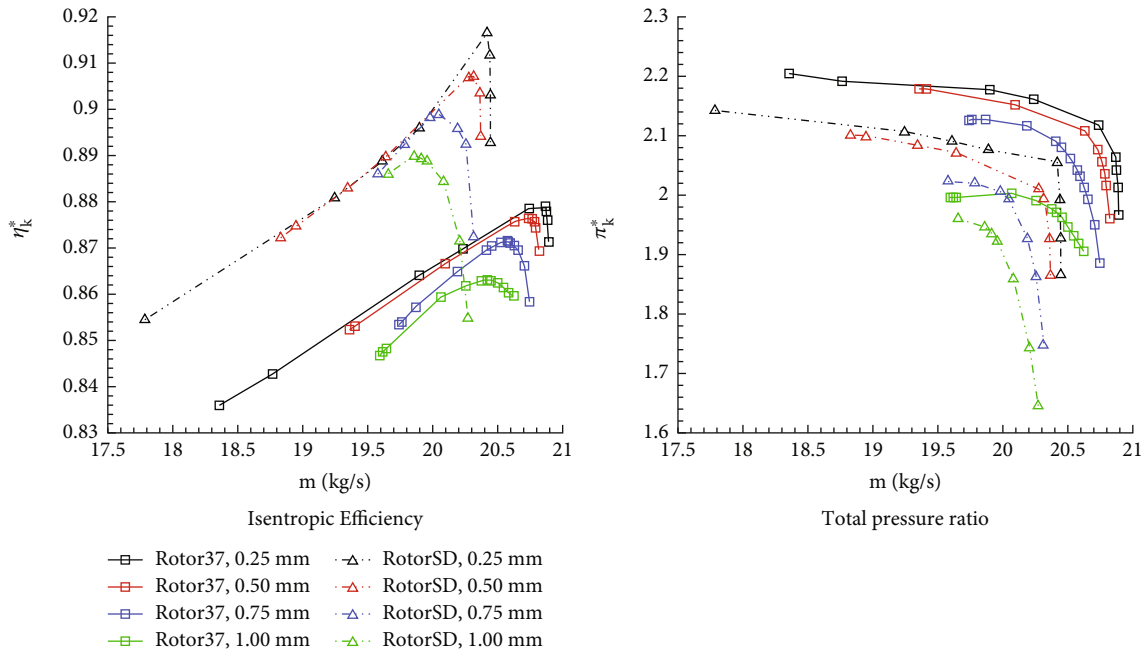

Figure 8: Comparison of the characteristics of the two rotors with different clearances.

respectively (see Figure 3), and N_j is the number of spanwise nodes. Figure 7 shows that when the number of grid cells is more than 610,000, the calculation results almost do not change with the number of grid cells [29]. Therefore, a grid with 610,000 grid cells is used in this paper.

4. Effect of the Tip Clearance on the Aerodynamic Performance of the Two Rotors

The blade tip clearances of Rotor37 and RotorSD were set to 0.25 mm, 0.50 mm, 0.75 mm, and 1.00 mm, and the effects of the blade tip clearances on the aerodynamic performance of the two rotors and flow fields in the tip regions were analyzed by numerical calculation.

Figure 8 shows that the total pressure ratio, isentropic efficiency, and mass flow rate of the two rotors decrease with increasing tip clearance in the whole flow rate range. The effect of the tip clearance on the values of the aerodynamic performance parameters is shown in Figure 9. Figure 9(a) shows the relationship between the tip clearance and the relative variation of the peak efficiency Δ_{EFF} (based on the efficiency at the tip clearance of 0.25 mm, Figures 8(c) and 8(d) and 9(b) are the same); Figure 9(b) shows the relationship between the tip clearance and relative variation of the peak

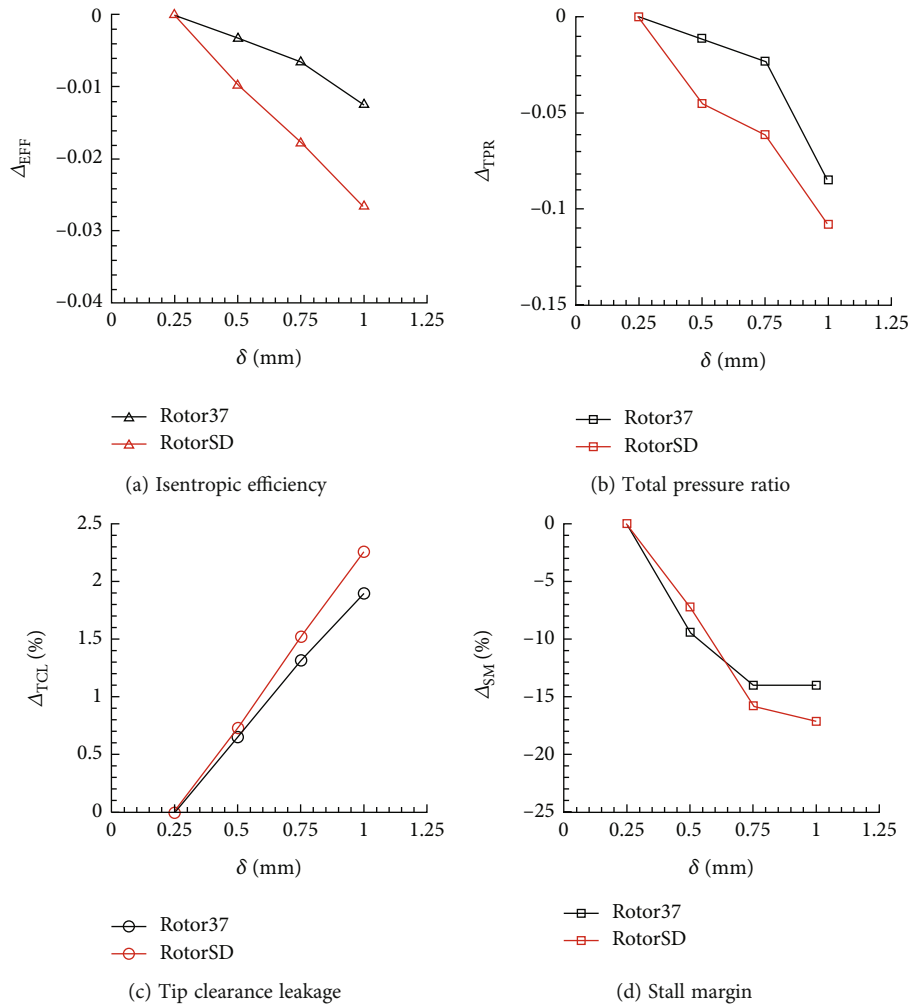

Figure 9: Comparison of the effect of the tip clearance on the performance of the two rotors.

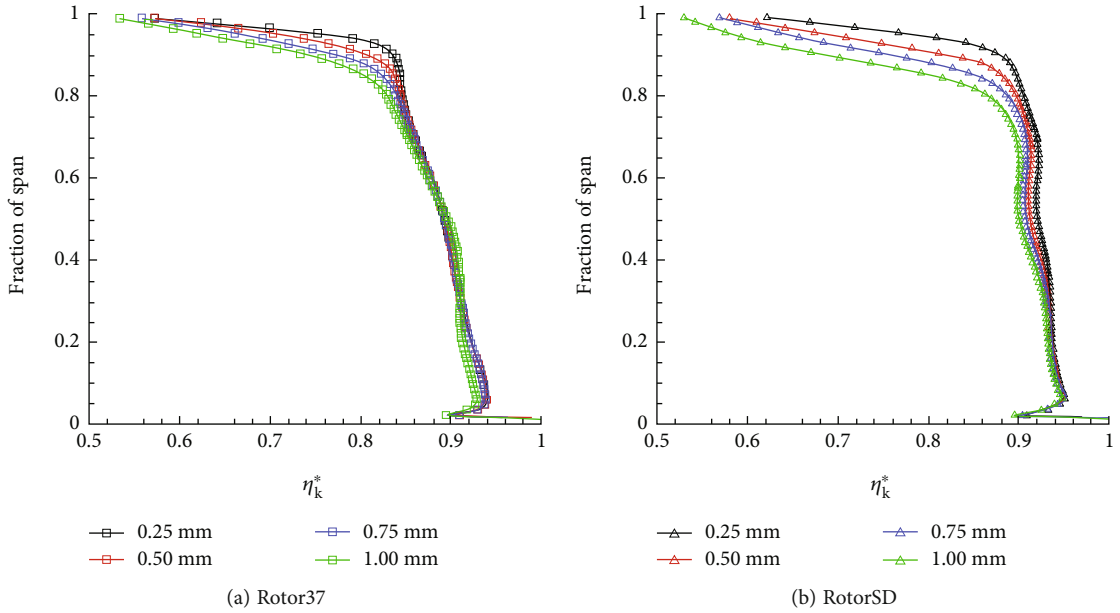

Figure 10: Isentropic efficiency distribution along the span.

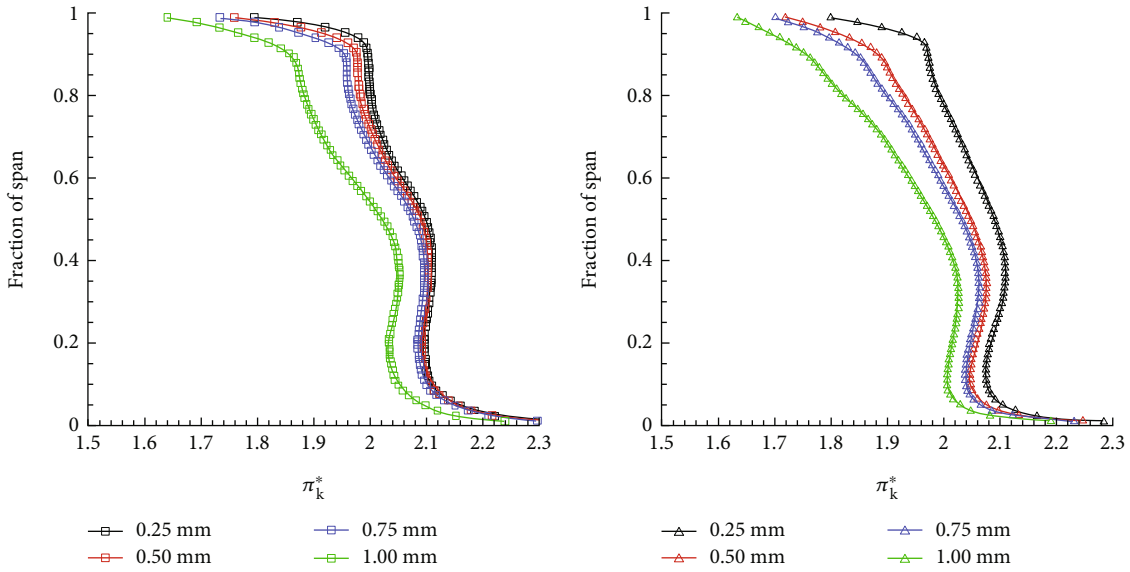

Figure 11: Total pressure ratio distribution along the span.

total pressure ratio Δ_{TPR}; Figure 9(c) shows the relationship between the tip clearance and the relative variation of the nondimensional flow rate of the tip clearance leakage Δ_{TCL} (ratio of the flow rate of the clearance leakage to the main flow rate); Figure 9(d) shows the relationship between the tip clearance and the relative variation of the stall margin. It can be seen from Figure 8 that with an increase in the tip clearance and a decrease in the isentropic efficiency, the total pressure ratio and the stall margin of RotorSD are more severe than those of Rotor37, and the leakage flow rate increases more. Therefore, with an increase in the tip clearance, the aerodynamic performance of RotorSD deteriorates more than that of Rotor37, although at the design point, the performance of the former is better than that of the latter. Figures 10 and 11 show that the efficiency and the total pressure ratio near the blade tip region of RotorSD decrease more than those of Rotor37 as the tip clearance increases.

5. Effect of the Tip Clearance on the Flow Fields near the Blade Tip at the Peak Efficiency Point

For the two rotors with tip clearances of 0.25 mm, 0.5 mm, 0.75 mm, and 1.0 mm, the relative Mach number contours of the S_1 surface at 90%, 94%, and 98% spans and at the middle of the tip clearance are shown in Figure 12. From the relative Mach number contours of the S_1 surface at the 90% span for Rotor37 at the tip clearance of 0.25 mm (seen in Figure 12(a)), the Mach number before the normal shock is 1.49; for RotorSD in the same tip clearance, the Mach number before the oblique shock is 1.47 and the Mach number before the ending normal shock is 1.3. Therefore, the intensities of the two shock waves at the 90% span of RotorSD are weaker than that of the normal shock wave at the 90% span of Rotor37. Additionally, from Figure 12(a), with the increase in the tip clearance, the shock wave structures of the two rotors are basically unchanged at the 90% span. Comparing Figures 12(a)–12(c), for the same rotor, the closer to the tip, the greater the change of shock wave intensity or structure with the increase of the clearance, and the change for Rotor37 is much less than that for RotorSD, which shows that the stronger the shock wave is, the less easily it is disturbed. At the peak efficiency point, the contours of entropy at 95% span and tip vortex structures in the tip fields of the two rotors at two tip clearances are shown in Figures 12 and 13, respectively. The Q in Figure 14 represents the second invariants of the velocity gradient tensor which defines as

$$Q = -\frac{1}{2} U_{ij} U_{ji} = \frac{1}{4} \left(\Omega_i \Omega_i - 2 S_{ij} S_{ij} \right), \tag{1}$$

where $U_{ij} = \partial u_i / \partial x_j$ is the velocity gradient tensor, $\Omega_i = \varepsilon_{ijk} \partial u_j / \partial x_k$ is the velocity field, and $S_{ij} = 1/2(\partial u_i / \partial x_j + \partial u_j / \partial x_i)$ is the rate-of-strain tensor. It can be seen from Figure 13 that with an increase of the clearance, the tip leakage mass flow rate increases, resulting in the increase in tip leakage vortex intensity especially the first tip leakage vortex intensity (shown in Figure 14), which cause more low-momentum fluid accumulates in the pressure sides (shown in Figure 13). From Figure 8(c), the tip leakage mass flow rates of the two rotors at the minimal tip clearance are nearly the same; but with the increase of the clearance, the increase of the tip leakage mass flow rate of RotorSD is greater than that of Rotor37. Therefore, the efficiency drop near the tip region of the RotorSD is greater than that of Rotor37(seen in Figure 11). However, the more shock waves there are, the weaker the intensity of each shock wave, and the more easily they are disturbed. Therefore, the greater the number of shock

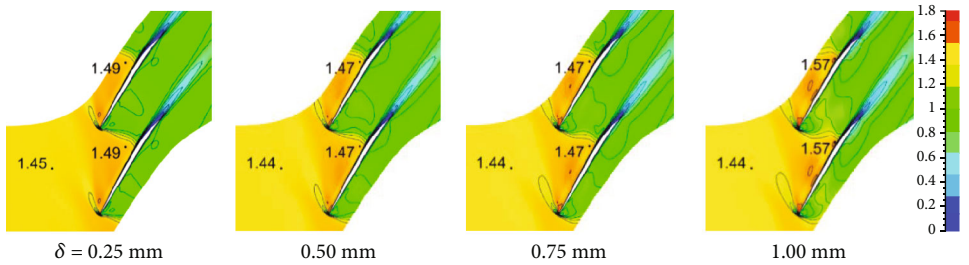

δ = 0.25 mm 0.50 mm 0.75 mm 1.00 mm

Rotor37

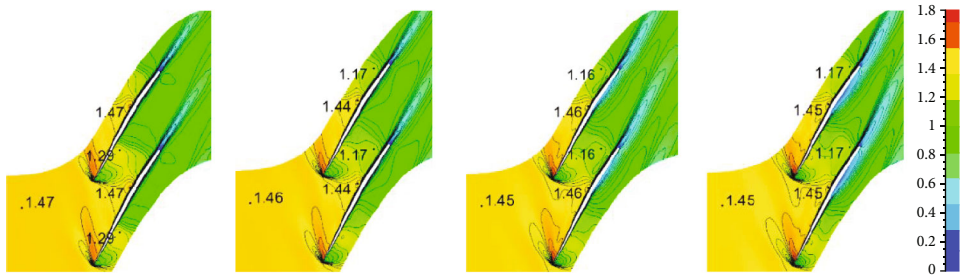

δ = 0.25 mm 0.50 mm 0.75 mm 1.00 mm

RotorSD

(a) 90% span

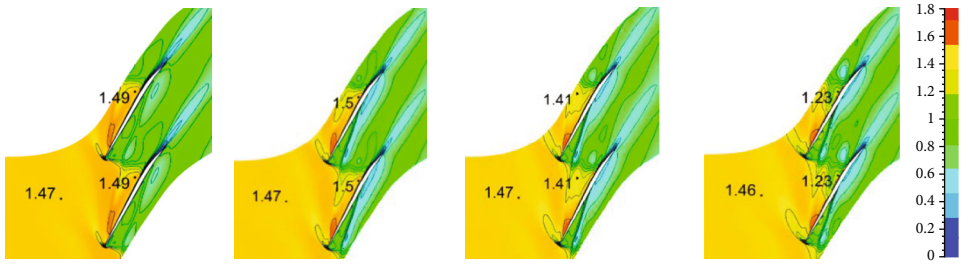

δ = 0.25 mm 0.50 mm 0.75 mm 1.00 mm

Rotor37

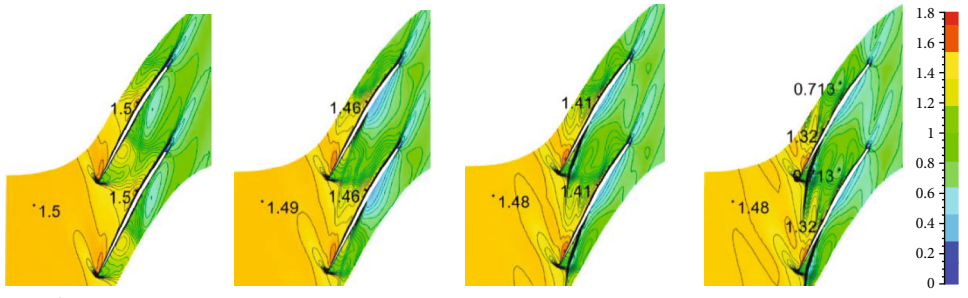

δ = 0.25 mm 0.50 mm 0.75 mm 1.00 mm

RotorSD

(b) 98% span

Figure 12: Continued.

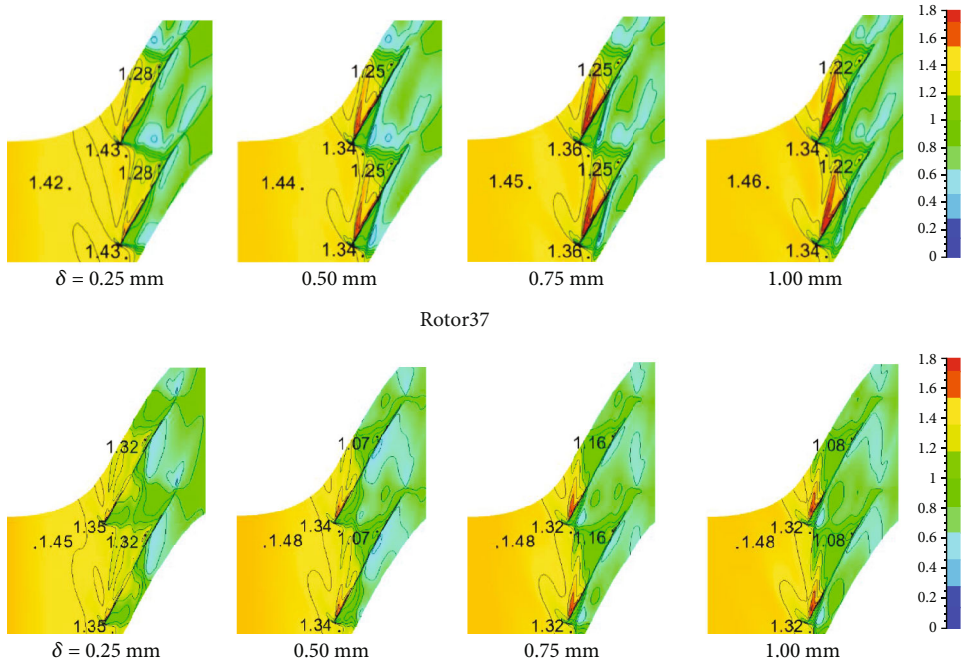

(c) Middle of the tip clearance

Figure 12: Contours of the relative Mach number.

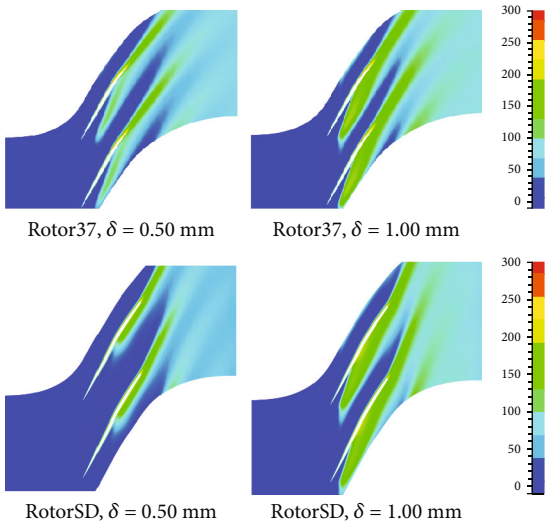

Figure 13: Contours of entropy (J/(kg·K)) in 95%span.

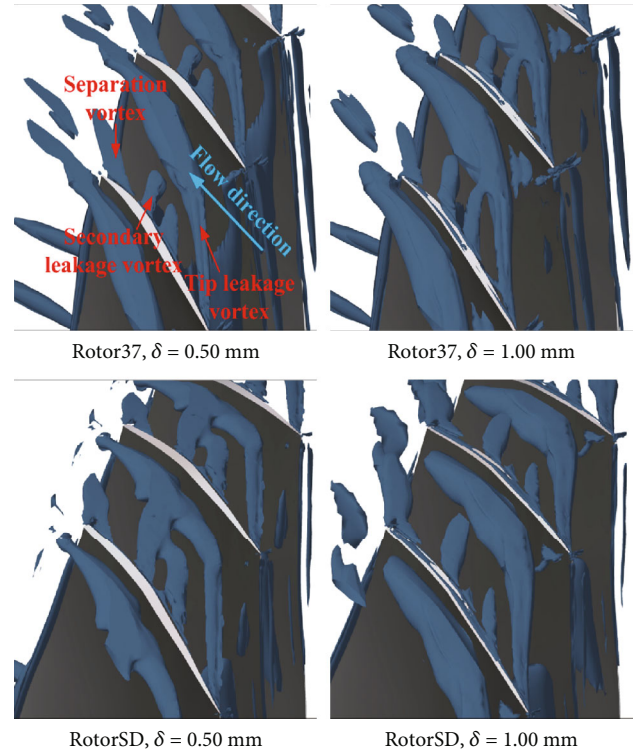

Figure 14: Tip vortex structure ($Q = 9 \times 10^7$).

waves is, the more sensitive the flow field near the blade tip is to the tip clearance, and the faster the performance decays as the tip clearance increases. Figures 15 and 16 show the entropy contours and streamlines near the blade tip of Rotor37 and RotorSD with the four tip clearances, respectively. The comparison between Figures 15 and 16 shows that with an increase in the tip clearance, the entropy increase of RotorSD is significantly greater than that of Rotor37.

To further verify that the decrease in aerodynamic performance of the two rotors with the increase of the tip clearance is mainly due to the change of shock waves, the rotation speed of the two rotors is reduced to 70% of the design speed (12032 rpm) to eliminate the channel

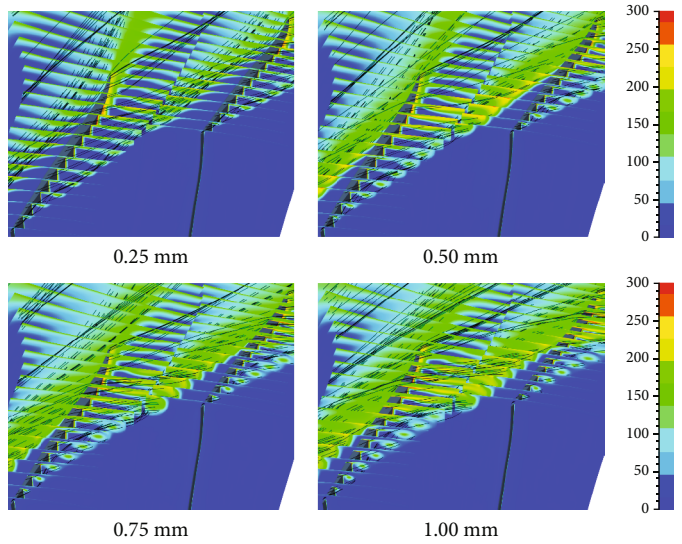

Figure 15: Contours of TCL streamlines and entropy near the blade tip of Rotor37.

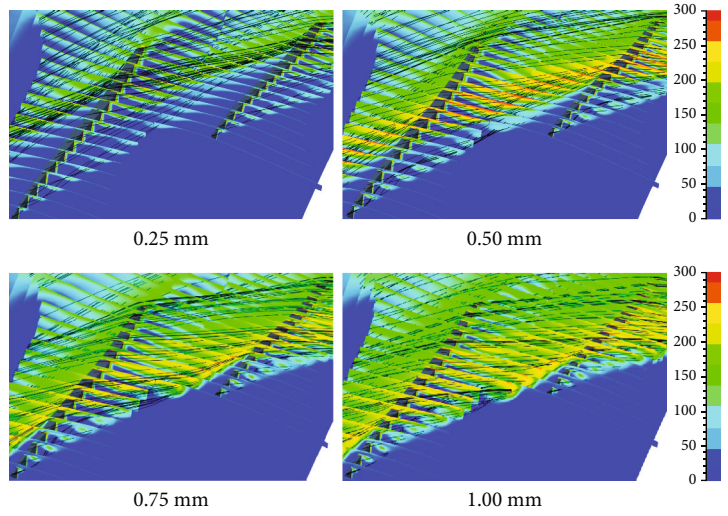

Figure 16: Contours of flow streamlines and entropy near the blade tip of RotorSD.

Table 3: Performance of the two rotors at 70% design speed.

Blade	δ (mm)	$\dot{m}$ (kg/s)	π_k^*	η_k^*	Δ_{EFF}	$\dot{m}_{\mathrm{leakage}}$ (%)
Rotor37	0.25	15.889	1.377	0.9173	/	0.51
	0.50	15.998	1.365	0.9171	-0.02%	0.99
	0.75	15.994	1.363	0.9157	-0.14%	1.50
	1.00	15.904	1.359	0.9142	-0.29%	2.03
RotorSD	0.25	14.651	1.318	0.8884	/	0.49
	0.50	14.605	1.317	0.8883	-0.01%	1.03
	0.75	14.593	1.314	0.8881	-0.02%	1.63
	1.00	14.567	1.311	0.8877	-0.06%	2.27

shock waves of the two rotors, and the effect of the increase of the blade tip clearance on the performance of the two rotors is investigated. The overall performance comparison of the two rotors at 70% of the design speed is shown in Table 3. The efficiency variation Δ_{EFF} of the two rotors with the tip clearance is very small at low speeds without shock waves near the blade tip region. From Figures 17 and 18, the distributions of the efficiency and total pressure ratio along the span also vary very

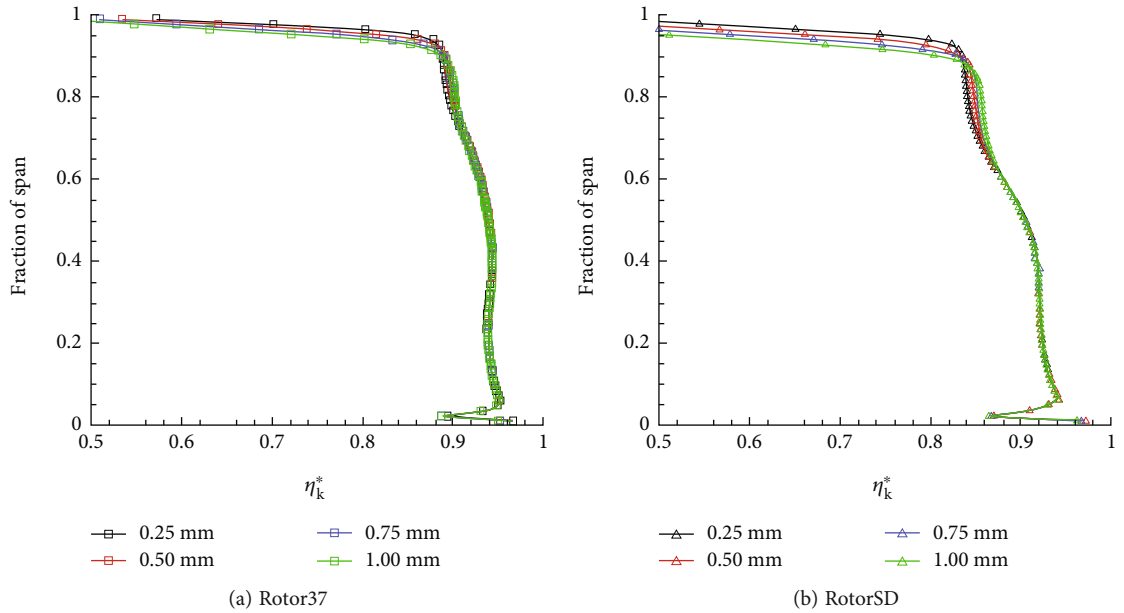

Figure 17: Distribution of the isentropic efficiency along the span at 70% of the design speed.

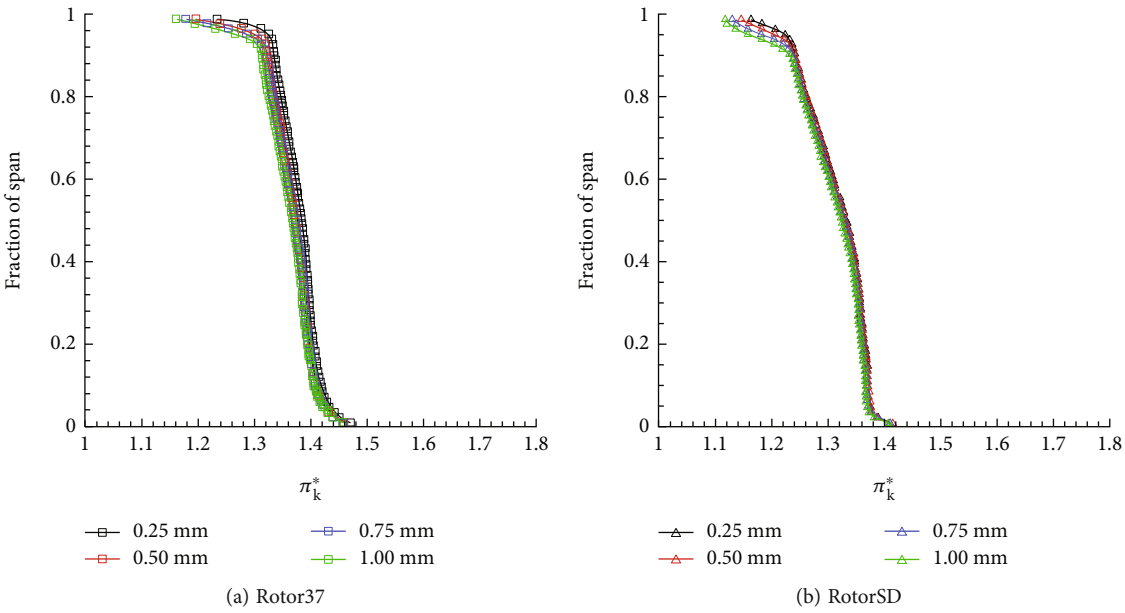

Figure 18: Distribution of the total pressure ratio along the span at 70% of the design speed.

little with increasing tip clearance. From Figure 19, there is no shock wave in the passages at the 90% span for both two rotors. These results support the above argument from the negative side: as the tip clearance increases, the decrease in the aerodynamic performance of the rotors is mainly due to changes in the shock waves.

6. Driving Factors of the Tip Clearance Leakage Flow

The tip clearance leakage flow is the main factor causing the increase in flow loss in the tip area. The above results show that the tip clearance leakage flow rate varies linearly with the tip clearance size at the design rotating speed and 70% of the design rotating speed (seen in Table 3). Therefore, the leakage flow rate per unit flow area at different clearance sizes is unchanged. In the following, the driving factors of leakage flow per unit flow area are demonstrated.

As shown in Figure 20, A represents a microelement of the tip clearance area at a certain chord position, which is composed of n mesh cells, and ρ_i, W_{ni}, and ΔA_i represent the flow density at the ith cell, the relative velocity perpendicular to the cell, and the area of the cell, respectively. $\bar{\dot{m}}_{\text{leakage}}$ represents the average value of the leakage flow rate

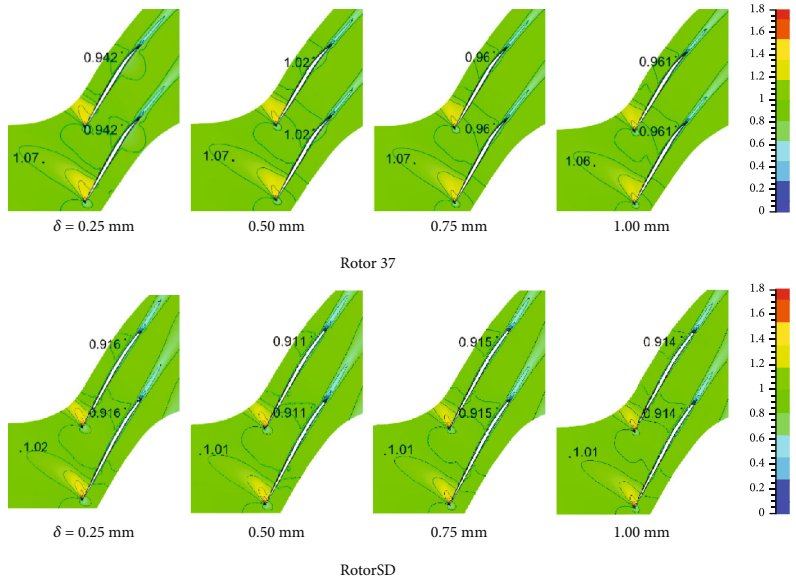

Figure 19: Contours of the relative Mach number at 70% of the design speed.

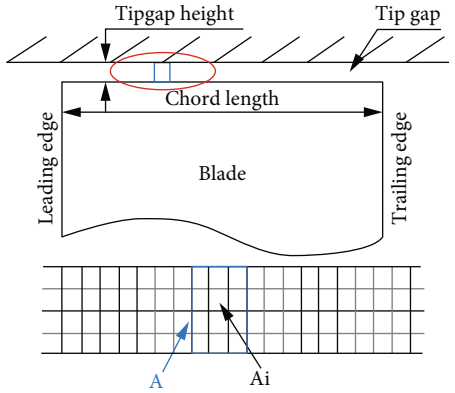

Figure 20: Schematic of parameter definitions at the tip clearance.

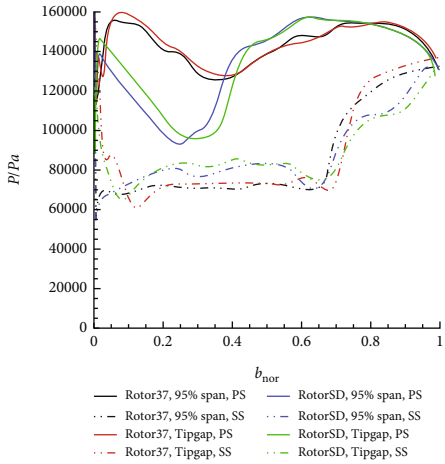

Figure 21: Distributions of the static pressures on the pressure and suction surfaces at the 95% span and along the chord.

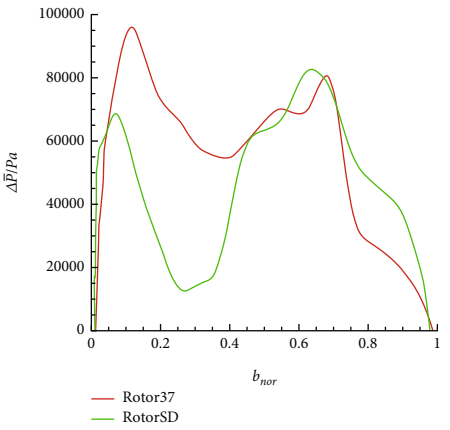

Figure 22: Pressure differences between the pressure and suction sides of the clearances along the chords at a tip clearance of 0.25 mm.

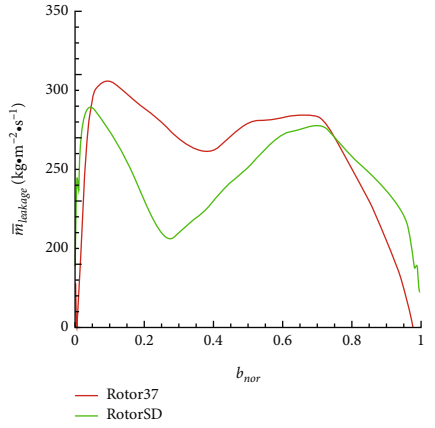

Figure 23: Distributions of the average leakage flow rate at a tip clearance of 0.25 mm.

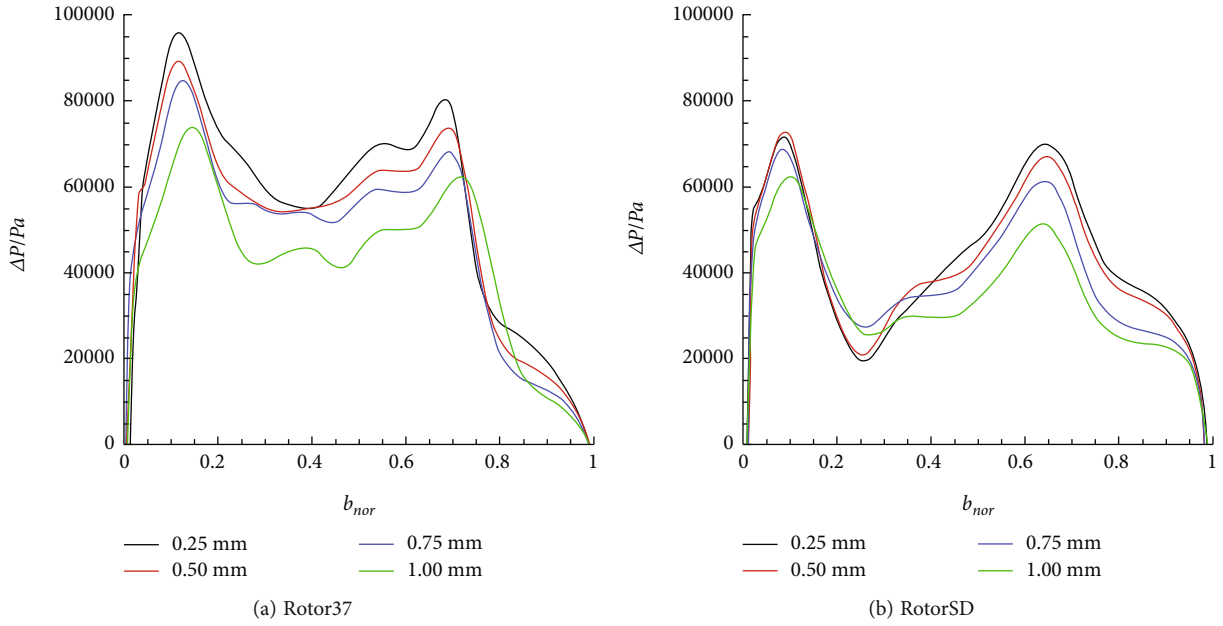

(a) Rotor37 (b) RotorSD

Figure 24: Pressure differences between the pressure and suction sides of the clearances along the chords at the four tip clearances.

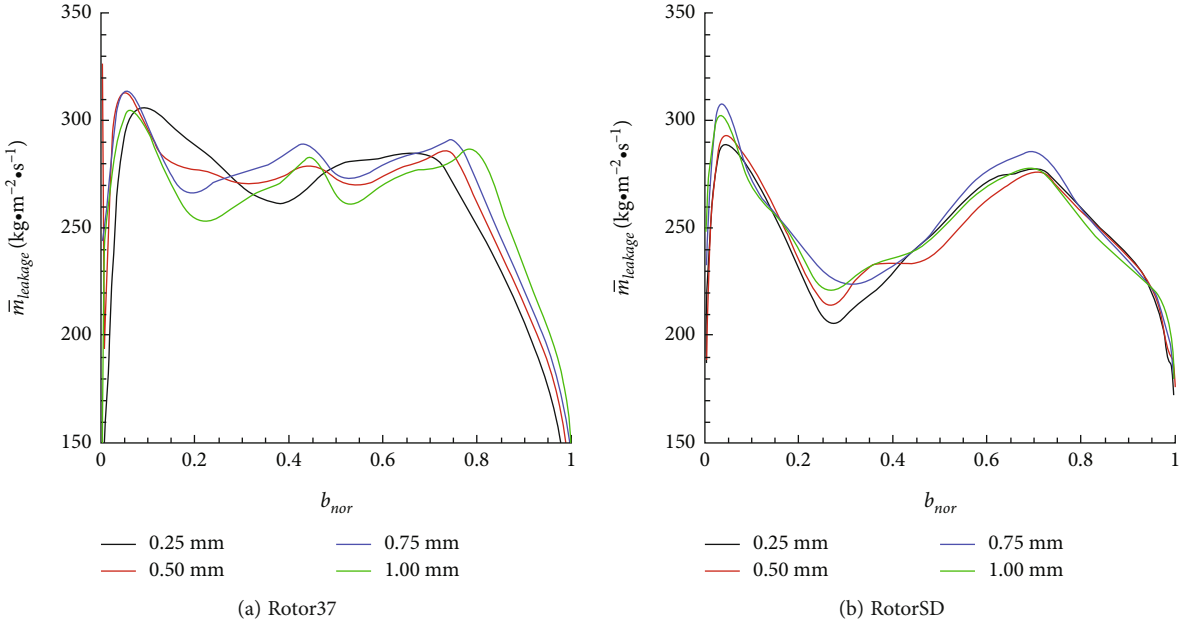

(a) Rotor37 (b) RotorSD

Figure 25: Distributions of the average leakage flow rate at the four tip clearances.

per unit area at the position, and $\Delta\bar{P}$ represents the average value of the pressure difference between the pressure and suction sides of the clearance, which are defined as

$$\dot{\bar{m}}_{\text{leakage}} = \frac{\sum_{i=1}^{n} \rho_i W_{ni} \Delta A_i}{\sum_{i=1}^{n} \Delta A_i}, \qquad \Delta\bar{P} = \bar{P}_{\text{PS}} - \bar{P}_{\text{SS}}. \tag{2}$$

$\bar{P}_{\text{PS}}$ and $\bar{P}_{\text{SS}}$ are the average pressures on the pressure surface and the suction sides in the tip clearance at the same chord position, respectively, and the average pressure is defined as

$$\bar{P} = \frac{\sum_{i=1}^{n} \rho_i W_{ni} P_i \Delta A_i}{\sum_{i=1}^{n} \rho_i W_{ni} \Delta A_i}. \tag{3}$$

For the two rotors with a clearance of 0.25 mm, the distributions of the static pressures on the pressure and suction surfaces at the 95% span and $\bar{P}_{\text{PS}}$ and $\bar{P}_{\text{SS}}$ (the average pressure on the pressure surface and suction sides, respectively, at the tip clearance) along the chord are shown in Figure 21. Figure 21 shows that the static pressures on both

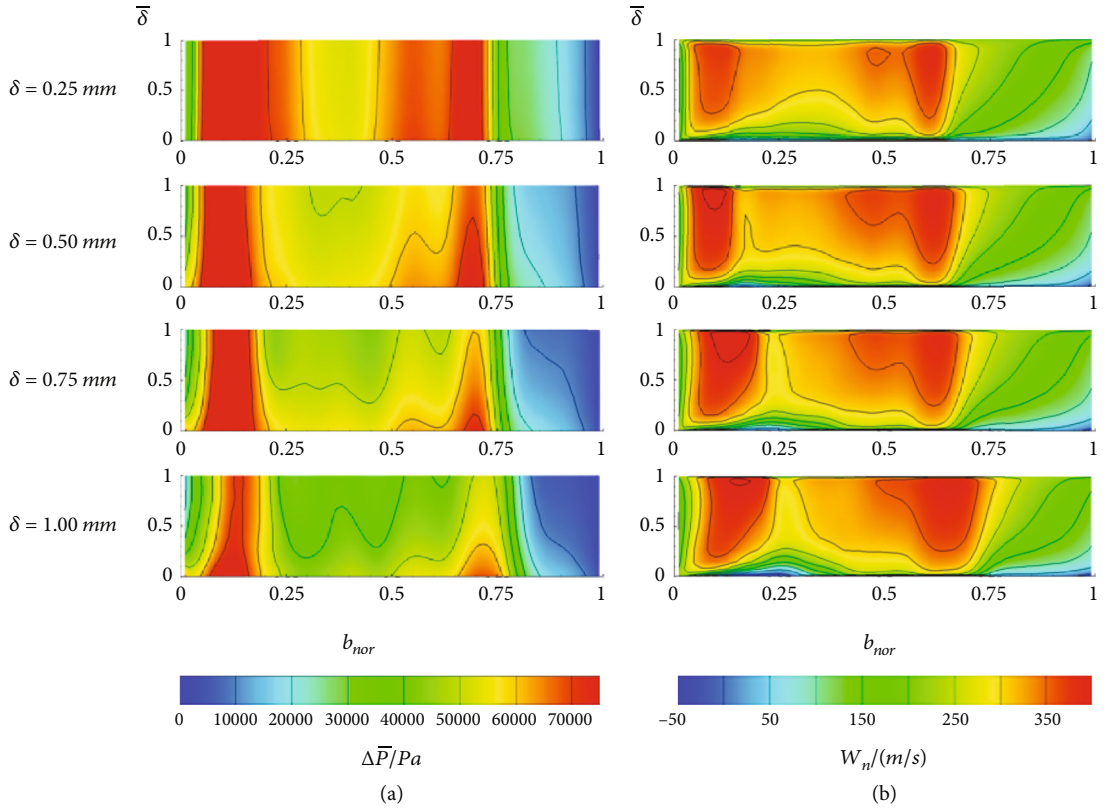

Figure 26: Distribution of flow parameters at the tip clearance of Rotor37. (a) Distributions of the pressure difference. (b) Distributions of relative velocity perpendicular to the pressure surface at the blade tip.

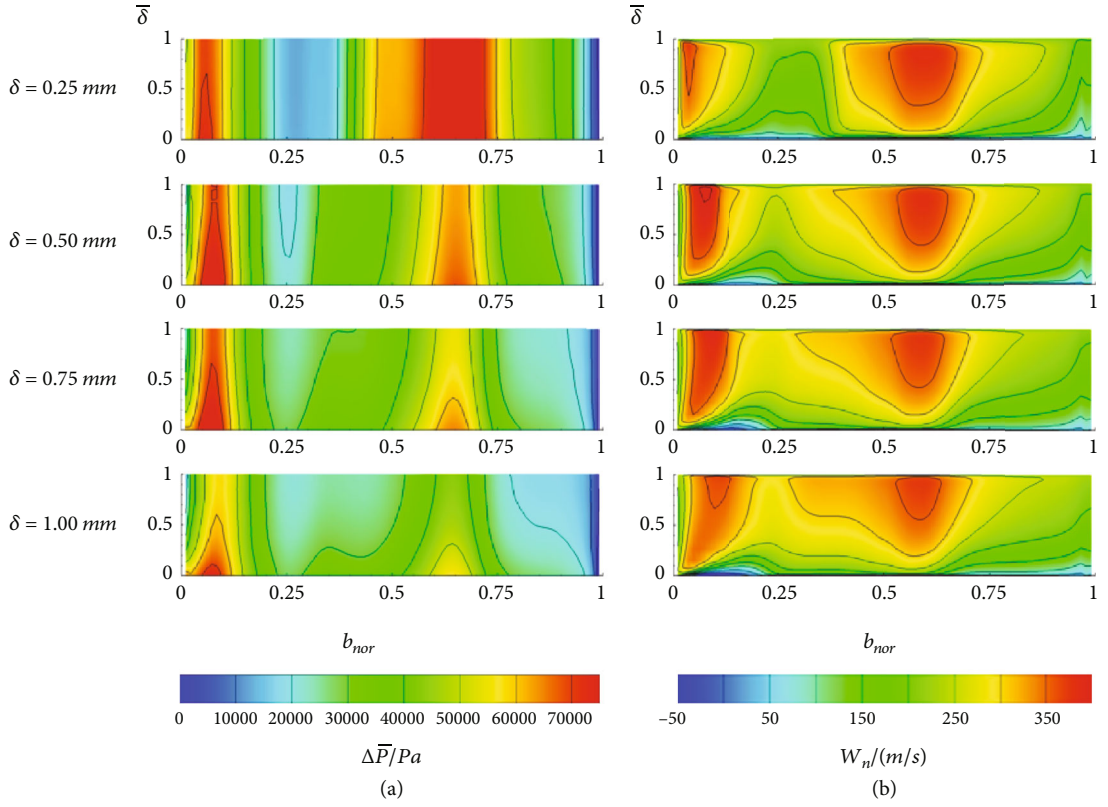

Figure 27: Distribution of the flow parameters at the tip clearance of RotorSD. (a) Distributions of the pressure difference. (b) Distributions of relative velocity perpendicular to the pressure surface at the blade tip.

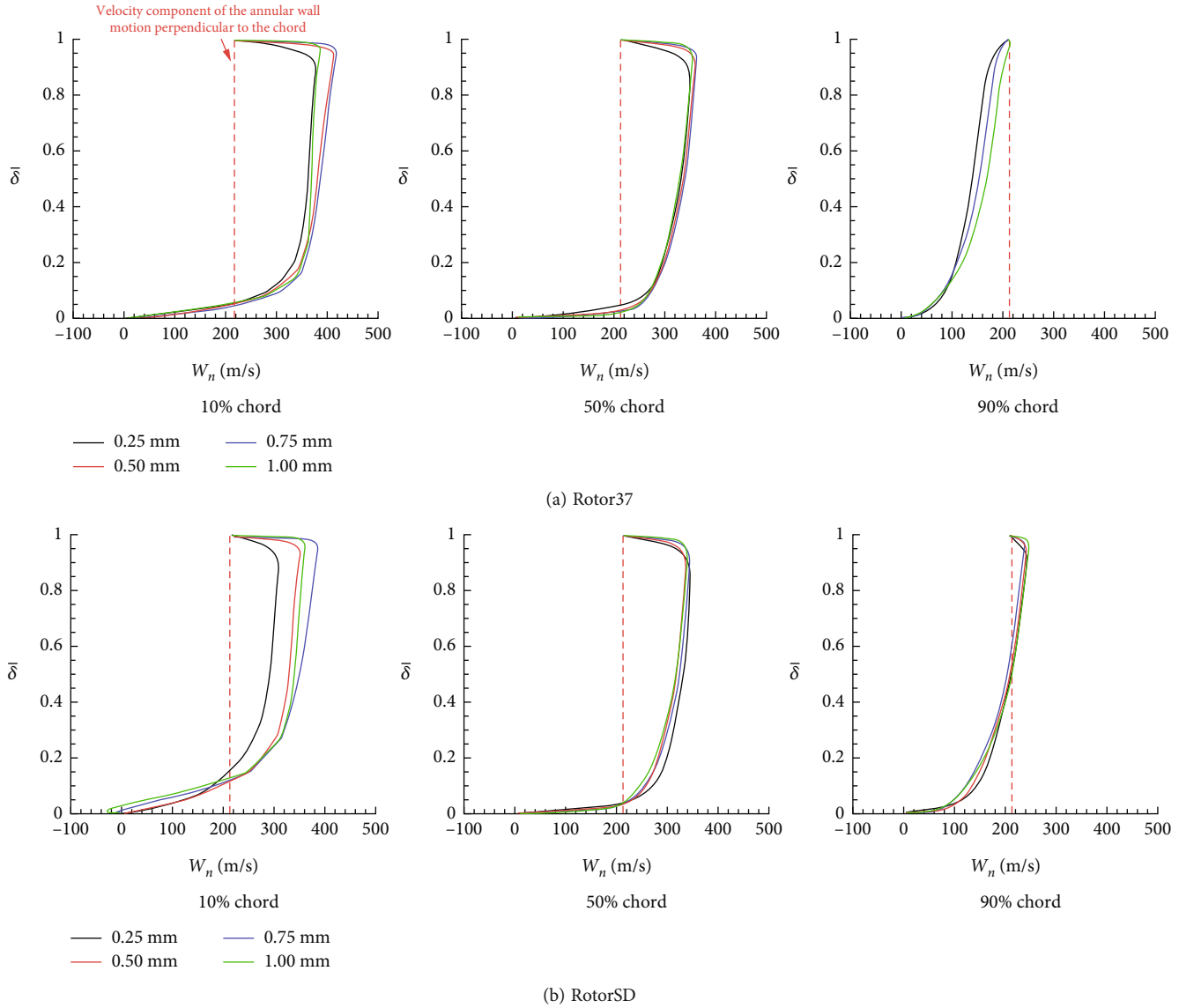

Figure 28: Distribution of the normal velocity along the gap height at 10%, 50%, and 90% chord lengths.

sides of the tip clearance are nearly equal to the static pressures of the corresponding sides at the 95% span. Figures 22 and 23 show distributions of the average pressure difference between the pressure and suction sides of the clearances $\Delta\bar{P}$ and the average leakage flow rate per unit area $\bar{\dot{m}}_{\text{leakage}}$ along the chord for the two rotors with a clearance of 0.25 mm. Comparing the two figures, the variation trend of $\Delta\bar{P}$ is the same as that of $\bar{\dot{m}}_{\text{leakage}}$, indicating that the pressure difference is one of the main driving forces of the tip leakage flow. Figures 24 and 25 show that the distributions of $\Delta\bar{P}$ and $\bar{\dot{m}}_{\text{leakage}}$ along the chord are affected quite slightly by the tip clearance, so the total leakage flow rate changes linearly with the size of the tip clearance.

Figures 26 and 27 show the contours of the pressure difference $\Delta\bar{P}$ and relative velocity perpendicular to the pressure surface at the blade tip W_n, where $\bar{\delta}$ is the dimensionless tip clearance, 0 for the blade surface and 1 for the annular wall. From Figures 26(a) and 27(a), when the tip clearance is small, the isopleths of $\Delta\bar{P}$ are approximately perpendicular to the annular wall and the blade tip end surface, indicating that the flow in the clearance is approximately parallel to the annular wall and blade tip end surface, and the pressure gradient normal to the wall and the surface is approximately zero. As the tip clearance increases, the orthogonality between the contours of $\Delta\bar{P}$ near the blade tip end surface becomes weaker, but the orthogonality between the contours and the annular wall is still stronger. This result implies that as the tip clearance increases, the three-dimensionality of the tip clearance flow near the blade tip end becomes stronger, and the tip clearance flow near the annular wall is still approximately parallel to the wall. From Figures 26(b) and 27(b), as the tip clearance increases, the contours of the normal velocity W_n change little, which again shows that the leakage flow is approximately proportional to the tip clearance size.

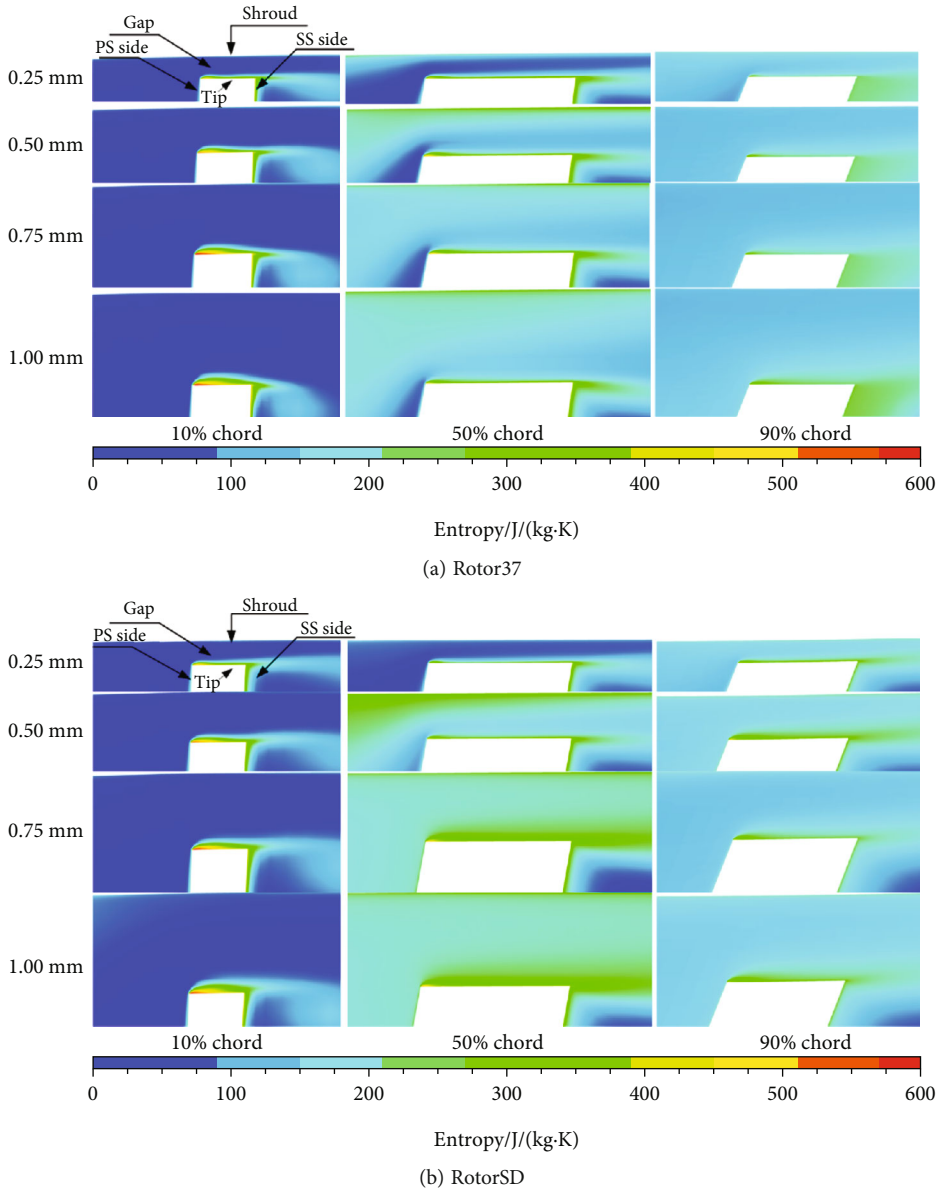

Figure 29: Contour of entropy at the tip clearances at 10%, 50%, and 90% chords.

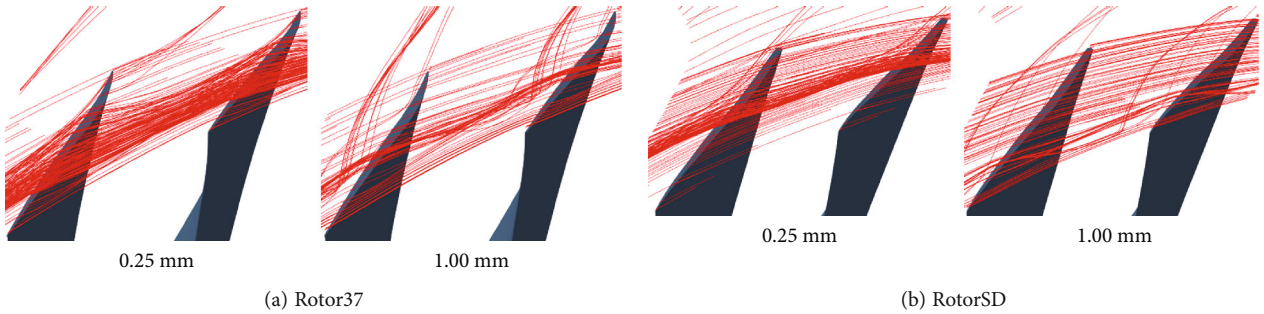

Figure 30: Leakage flow streamlines at 97% clearance height.

Comparing Figures 26(a) and 26(b) and 27(a) and 27(b), it can be seen that the region with a larger pressure difference $\Delta\bar{P}$ has a higher normal velocity W_n (larger leakage flow rate) and a region with a smaller $\Delta\bar{P}$ has a smaller W_n. However, there is inconsistency between the contours of $\Delta\bar{P}$ and W_n, especially W_n is quite large in the region near the blade trailing edges where $\Delta\bar{P}$ is close to 0. Therefore, there are other drivers for the leakage flow.

The relative movement direction of the annular wall is the same as the direction of the leakage flow. Due to the viscous effect of the boundary layer attached to the wall, the leakage flow in the blade tip clearance is affected. Figure 28 shows the distribution of the normal velocity W_n along the tip height at 10%, 50%, and 90% chords. It can be seen from the figure that the tip clearance has little effect on the distribution of W_n. This result is consistent with the above results that the leakage flow rate is proportional to the blade tip clearance size. It can also be seen from Figure 28 that the velocity component of the annular wall motion perpendicular to the chord is smaller than the normal velocity W_n slightly away from the wall. Therefore, the annular wall motion has a blocking effect on the tip leakage flow; however, as seen from the figure, the affected region is small. Figure 29 shows that the increase in entropy in the tip clearance is very small, which implies that the flow in the tip clearance is low loss. From the above analysis, it can be concluded that the relative movement of the annular wall can reduce the leakage flow, but the effect is small.

The leakage flow streamlines at 97% clearance height under the minimum and maximum tip clearances (0.25 mm and 1.00 mm) are shown in Figure 30. There is an obvious double-leakage tip clearance flow (that is, the leakage flow generated by adjacent blades flows into the local tip clearance [21, 27, 30]). At the same time, Figures 15 and 16 show that there is a secondary leakage phenomenon in the leakage flow. This means that the tip clearance leakage flow is driven not only by the local tip pressure difference but also by the adjacent blade tip pressure difference, which leads to inconsistency between the contours of the pressure difference $\Delta\bar{P}$ and the normal velocity W_n in Figures 26 and 27.

7. Conclusion

The existence of tip leakage flow in a compressor rotor has a great impact on the aerodynamic performance of the compressor. This paper focuses on the tip clearance flows of two transonic rotors with the same design index but different shock wave structures. The following conclusions are drawn through the analysis of their aerodynamic performances and flow field characteristics via a numerical calculation method:

(1) For supersonic and transonic rotors, achieving the same total pressure ratio at the design point, the more shock waves in the flow field near the blade tip, the weaker the intensity of each shock wave, and the more easily they are disturbed. The efficiency of the rotor with a normal shock wave is lower than that of the rotor with two or more shock waves because the shock loss of the former is larger than that of the latter. However, the greater the number of shock waves, the more sensitive the flow field near the blade tip is to the tip clearance, and the faster the performance decays as the clearance increases

(2) The pressure difference between the pressure and suction sides of the tip clearance is the only driving factor for the tip clearance leakage flow. The leakage flow depends not only on the local pressure difference but also on the secondary tip leakage generated by adjacent blades. Although the movement direction of the annular wall is the same as the direction of the leakage flow, the movement speed of the annular wall is lower than the leakage flow speed, which has a minor blocking effect on the tip clearance leakage flow

(3) With an increase in the tip clearance, between the pressure and suction sides of the tip clearance, the static pressure difference and the leakage flow rate per unit area along the chord direction change little. Therefore, the total leakage flow rate changes linearly with the size of the tip clearance

Nomenclature

b: Chord
$\dot{m}$: Mass flow rate (kg/s)
$\dot{m}_{\text{leakage}}$: Total leakage mass flow (kg/s)
$\dot{m}_{\Delta P}$: Leakage mass flow by static pressure difference (kg/s)
N: Grid point number
P: Static pressure (Pa)
Q: The second invariants of the velocity gradient tensor
S: Entropy (J/(kg K))
u, v, w: Three components of velocity
W: Relative velocity (m/s)
η_k^*: Isentropic efficiency at the peak efficiency point
π_k^*: Total pressure ratio at the peak efficiency point
δ: Tip clearance (mm)
$\bar{\delta}$: Height at tip clearance, nondimensionalized by tip clearance.

Superscripts

$\bar{()}$: Surface average.

Subscripts

i, j, k: Azimuthal direction, spanwise direction, and streamwise direction of mesh, respectively
n, t, r: Normal, tangential, and radial directions, respectively, relative to the chord
1, 2: Inlet and outlet of tip clearance
nor: Normalized
EFF: Isentropic efficiency
TPR: Total pressure ratio
TCL: Tip clearance leakage, nondimensionalized by inlet mass flow
SM: Surge margin
PS: Pressure surface side
SS: Suction surface side.

Data Availability

The data that support the findings of this study are available from the corresponding author upon reasonable request.

Conflicts of Interest

The authors declares that they have no conflicts of interest.

Acknowledgments

This work was supported by the National Science and Technology Major Project (2017-II-0001-0013).

References

[1] K. L. Suder, "Blockage development in a transonic,axial compressor rotor," *Journal of Turbomachinery*, vol. 120, no. 3, pp. 465–476, 1998.

[2] D. Zhang, W. Shi, S. Wu, D. Pan, P. Shao, and H. Wang, "Numerical and experimental investigation of tip leakage vortex trajectory in an axial flow pump," in *Proceedings of the asme fluids engineering division summer meeting, 2013, VOL 1B: Symposia*, Incline Village, Nevada, USA, 2014.

[3] A. Jaatinen, T. Turunen-Saaresti, A. Grönman, P. Röyttä, and J. Backman, "Experimental study of the effect of the tip clearance to the diffuser flow field and stage performance of a centrifugal compressor," in *Proceedings of the ASME turbo EXPO 2012, VOL 8, PTS A-C*, pp. 641–648, Copenhagen, Denmark, 2012.

[4] J. Du, F. Lin, J. Chen, C. Nie, and C. Biela, "Flow structures in the tip region for a transonic compressor rotor," *Journal of Turbomachinery-Transactions of the ASME*, vol. 135, no. 3, 2013.

[5] B. Roy, A. M. Pradeep, A. Suzith, D. Bhatia, and A. Mulmule, "Study of tip flows in high hub-to-tip ratio axial compressors at low speed with varying tip gaps, inflow conditions and tip shapes," in *ASME Turbo Expo 2010: Power for Land, Sea, and Air*, Glasgow, UK, 2010.

[6] N. A. Cumpsty, *Compressor Aerodynamics*, Longman Scientific & Technical, 2004.

[7] M. Zhang, X. Dong, J. Li, D. Sun, and X. Sun, "Effect of differential tip clearance on the performance and noise of an axial compressor," *Aerospace Science and Technology*, vol. 132, article 108070, 2023.

[8] R. Zheng, J. Xiang, and J. Sun, "Blade geometry optimization for axial flow compressor," in *Proceedings of the ASME turbo EXPO 2010: Turbomachinery: axial flow fan and compressor aerodynamics design methods, and cfd modeling for turbomachinery, VOL 7, PTS A-C*, pp. 633–644, Glasgow, UK, 2010.

[9] C. Cao and Z. Zhai, "Influence of tip clearance on civil high-bypass-ratio transonic compressor aerodynamic performance," *Science Technology and Engineering*, vol. 19, pp. 230–236, 2019.

[10] T. F. Brooks, D. S. Pope, and M. A. Marcolini, "Airfoil self-noise and prediction," No. L-16528, 1989.

[11] M. Gennaro and H. Kuehnelt, "Broadband noise modelling and prediction for axial fans," in *International Conference on Fan noise, Technology and Numerical Methods*, Senlis (France), 2012.

[12] S. Sakulkaew, C. S. Tan, E. Donahoo, C. Cornelius, and M. Montgomery, "Compressor efficiency variation with rotor tip gap from vanishing to large clearance," *Journal of Turbomachinery*, vol. 135, no. 3, article 031030, 2013.

[13] F. Xie, W. L. Chu, X. J. Li, and C. L. Liu, "Influence of blade tip clearance at near-stall condition on transonic axial-flow compressor," *Journal of Aerospace Power*, vol. 29, pp. 2417–2423, 2014.

[14] B. Liu, X. Mao, P. Zhang, X. Q. Yang, and S. D. Xia, "Research on influence of tip clearance effects on transonic compressor performance," *Journal of Propulsion Technology*, vol. 37, pp. 1401–1410, 2016.

[15] S. N. Danish, S. U. R. Qureshi, M. M. Imran et al., "Effect of tip clearance and rotor-stator axial gap on the efficiency of a multistage compressor," *Applied Thermal Engineering*, vol. 99, pp. 988–995, 2016.

[16] A. Tiralap, C. S. Tan, E. Donahoo, M. Montgomery, and C. Cornelius, "Effects of rotor tip blade loading variation on compressor stage performance," *Journal of Turbomachinery*, vol. 139, no. 5, 2017.

[17] R. Matthias, L. Martin, and M. Ronald, "Investigation of performance and rotor tip flow field in a low speed research compressor with circumferential groove casing treatment at varying tip clearance," *International Journal of Rotating Machinery*, vol. 2017, Article ID 4631751, 14 pages, 2017.

[18] Z. Chen, Y. Wu, and G. An, "Tip leakage flow, tip aerodynamic loading and rotating instability in a subsonic high-speed axial flow compressor rotor," *Aerospace Science and Technology*, vol. 110, article 106486, 2021.

[19] R. Howard and S. L. Puterbaugh, "Performance impact of tip clearance variation on a transonic, low aspect ratio, axial compressor stage," in *50th AIAA/ASME/SAE/ASEE Joint Propulsion Conference*, Cleveland, OH, 2014.

[20] B. Liu, G. An, X. Yu, and Z. Zhang, "Experimental investigation of the effect of rotor tip gaps on 3D separating flows inside the stator of a highly loaded compressor stage," *Experimental Thermal and Fluid Science*, vol. 75, pp. 96–107, 2016.

[21] F. Lin and J. Chen, "Oscillatory tip leakage flows and stability enhancement in axial compressors," *International Journal of Rotating Machinery*, vol. 2018, Article ID 9076472, 14 pages, 2018.

[22] P. V. Ramakrishna and M. Govardhan, "Study of sweep and induced dihedral effects in subsonic axial flow compressor passages—part II: detailed study of the effects on tip leakage phenomena," *International Journal of Rotating Machinery*, vol. 2010, Article ID 491413, 13 pages, 2010.

[23] R. V. Chima, "Calculation of tip clearance effects in a transonic compressor rotor," *Journal of Turbomachinery*, vol. 120, no. 1, pp. 131–140, 1998.

[24] M. Hoeger, G. Fritsch, and D. Bauer, "Numerical simulation of the shock-tip leakage vortex interaction in a HPC front stage," *Journal of Turbomachinery*, vol. 121, no. 3, pp. 456–468, 1999.

[25] Z. Zhang, X. Yu, and B. Liu, "Characteristics of the tip leakage vortex in a low-speed axial compressor with different rotor tip gaps," in *Proceedings of the ASME turbo EXPO 2012, VOL 8, PTS A-C*, pp. 311–322, Copenhagen, Denmark, 2012.

[26] B. Wang, Y. Wu, F. Yang, and S. Spence, "Intermittent breakdown of the tip leakage vortex and the resultant flow unsteadiness in the tip-region of a subsonic compressor cascade," *Aerospace Science and Technology*, vol. 113, article 106679, 2021.

[27] Y. Liu and L. Tan, "Theoretical prediction model of tip leakage vortex in a mixed flow pump with tip clearance," *Journal of Fluids Engineering*, vol. 142, no. 2, p. 142, 2020.

[28] Y. Han and L. Tan, "Dynamic mode decomposition and reconstruction of tip leakage vortex in a mixed flow pump as turbine at pump mode," *Renewable Energy*, vol. 155, pp. 725–734, 2020.

[29] J. Liu and Z. Zhou, "Study of improving surge margin of a supersonic compressor stage," *Journal of Propulsion Technology*, vol. 40, pp. 1780–1791, 2019.

[30] E. Erler, *Axial Compressor Blade Design for Desensitization of Aerodynamic Performance and Stability to Tip Clearance, [Ph.D. Thesis]*, École Polytechnique de Montréal, 2012.